iScience, Volume *24*

Supplemental information

Modeling SARS-CoV-2 infection and its individual differences with ACE2-expressing human iPS cells

Emi Sano, Sayaka Deguchi, Ayaka Sakamoto, Natsumi Mimura, Ai Hirabayashi, Yukiko Muramoto, Takeshi Noda, Takuya Yamamoto, and Kazuo Takayama

Supplemental figures

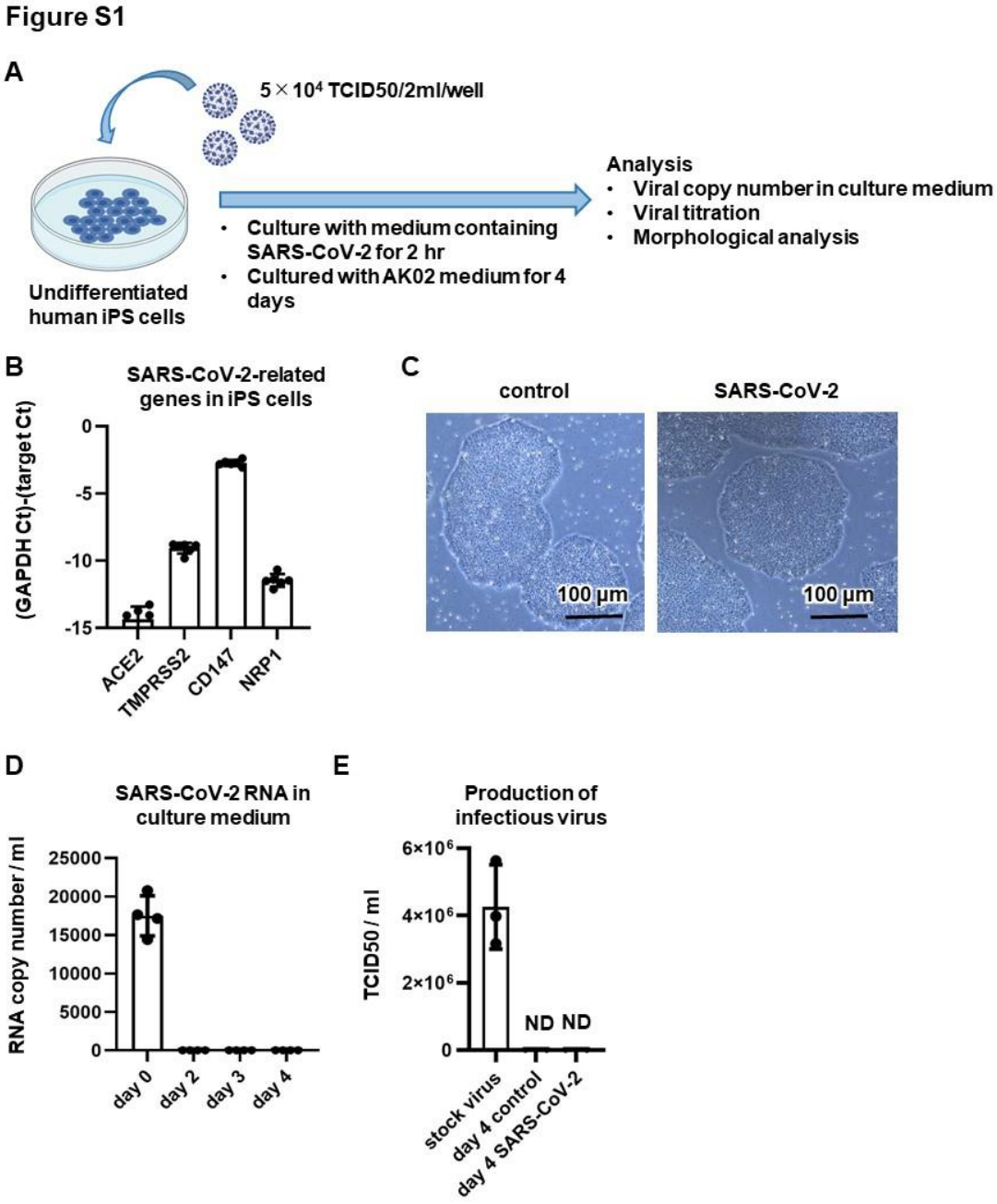

Figure S1 SARS-CoV-2 cannot infect human iPS cells, Related to Figure 1

(**A**) Undifferentiated human iPS cells (1383D6) were infected with SARS-CoV-2 (5×10^4 TCID50/well) for 2 hr and then cultured with AK02 medium for 4 days. (**B**) The gene expression levels of *ACE2*, *TMPRSS2*, *CD147*, and *NRP1* in human iPS cells were examined by qPCR. (**C**) Phase images of uninfected and infected human iPS cells are shown. (**D**) At days 0, 2, 3 and 4 after the infection, the viral RNA copy number in the

cell culture supernatant was measured by qPCR. day 0 = medium containing initial virus (5×104 TCID50/2ml). (**E**) The amount of infectious virus in the supernatant was measured by the TCID50 assay. Data are represented as means ± SD (*n*=3). ND=not detected.

Figure S2

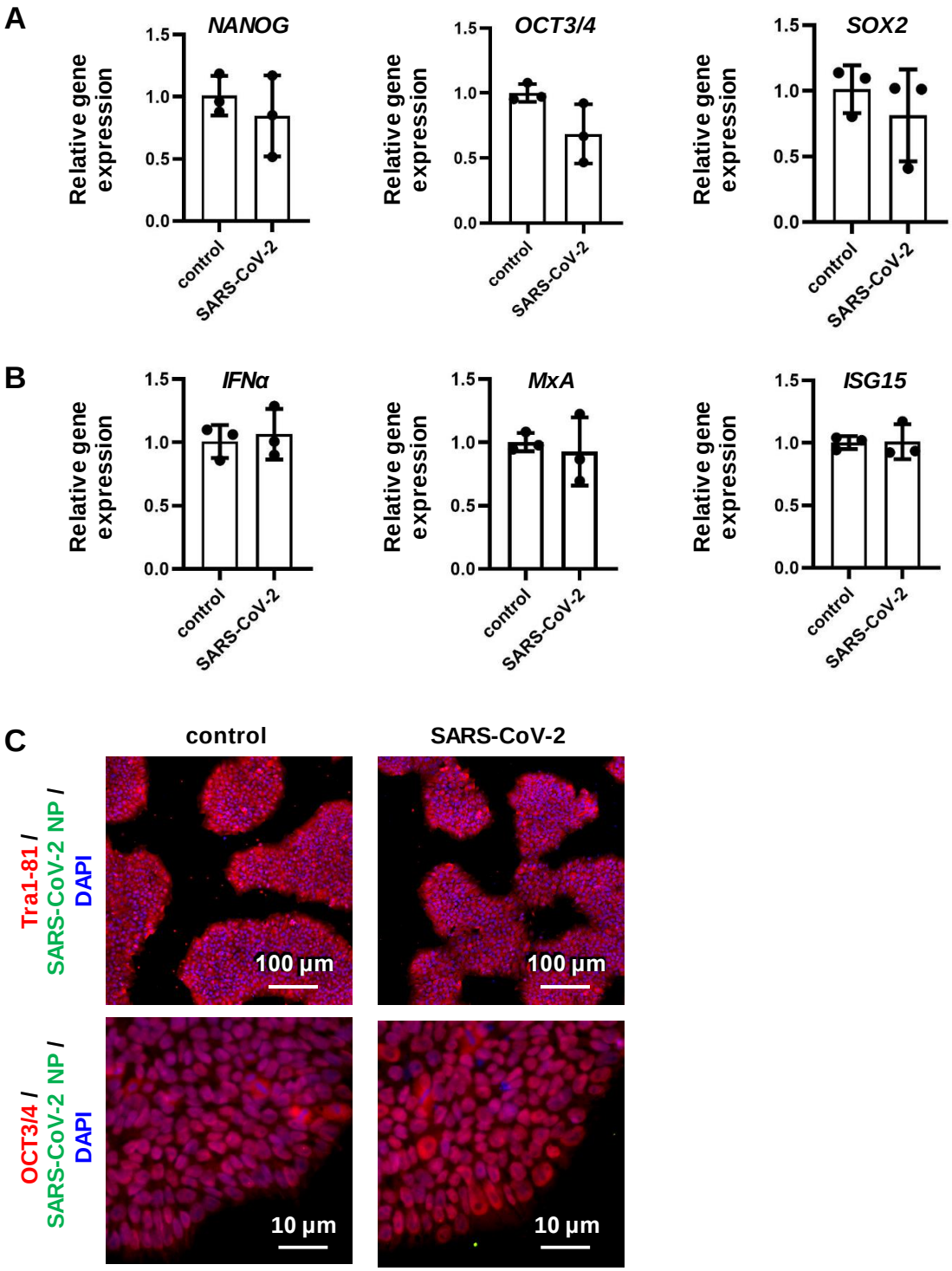

Figure S2 The pluripotent state of human iPS cells is not affected by SARS-CoV-2 infection, Related to Figure 1

The gene expression levels of pluripotent markers (*NANOG*, *OCT3/4*, and *SOX2*) (**A**) and innate immunity-related markers (*IFNα*, *MxA*, and *ISG15*) (**B**) in uninfected and infected human iPS cells were examined by qPCR. (**C**) Immunofluorescence analysis of SARS-CoV-2 NP (green), Tra1-81 (red), and OCT3/4 (red) in uninfected and infected human iPS cells. Nuclei were counterstained with DAPI (blue). Data are represented as means ± SD (*n*=3).

Figure S3

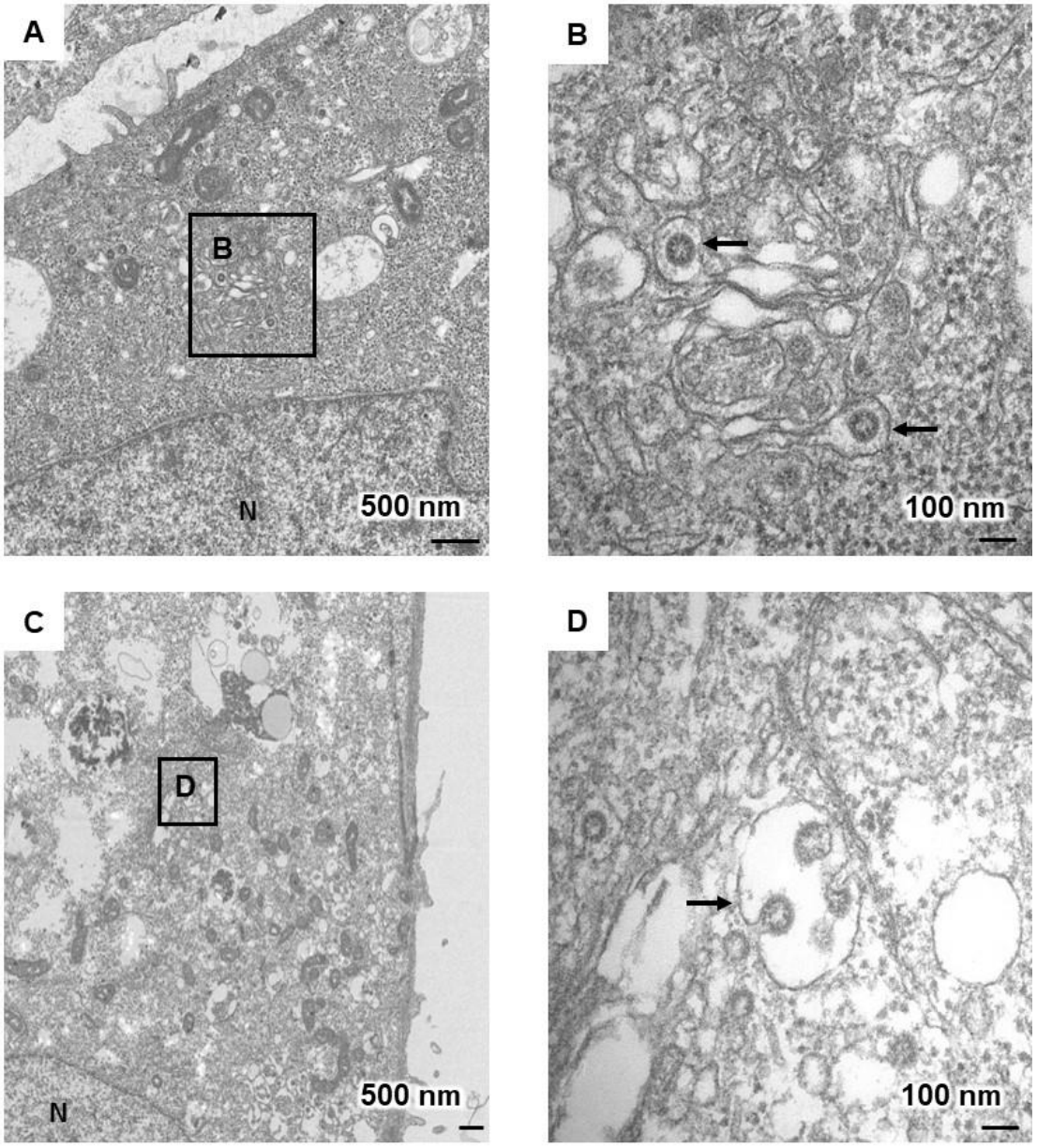

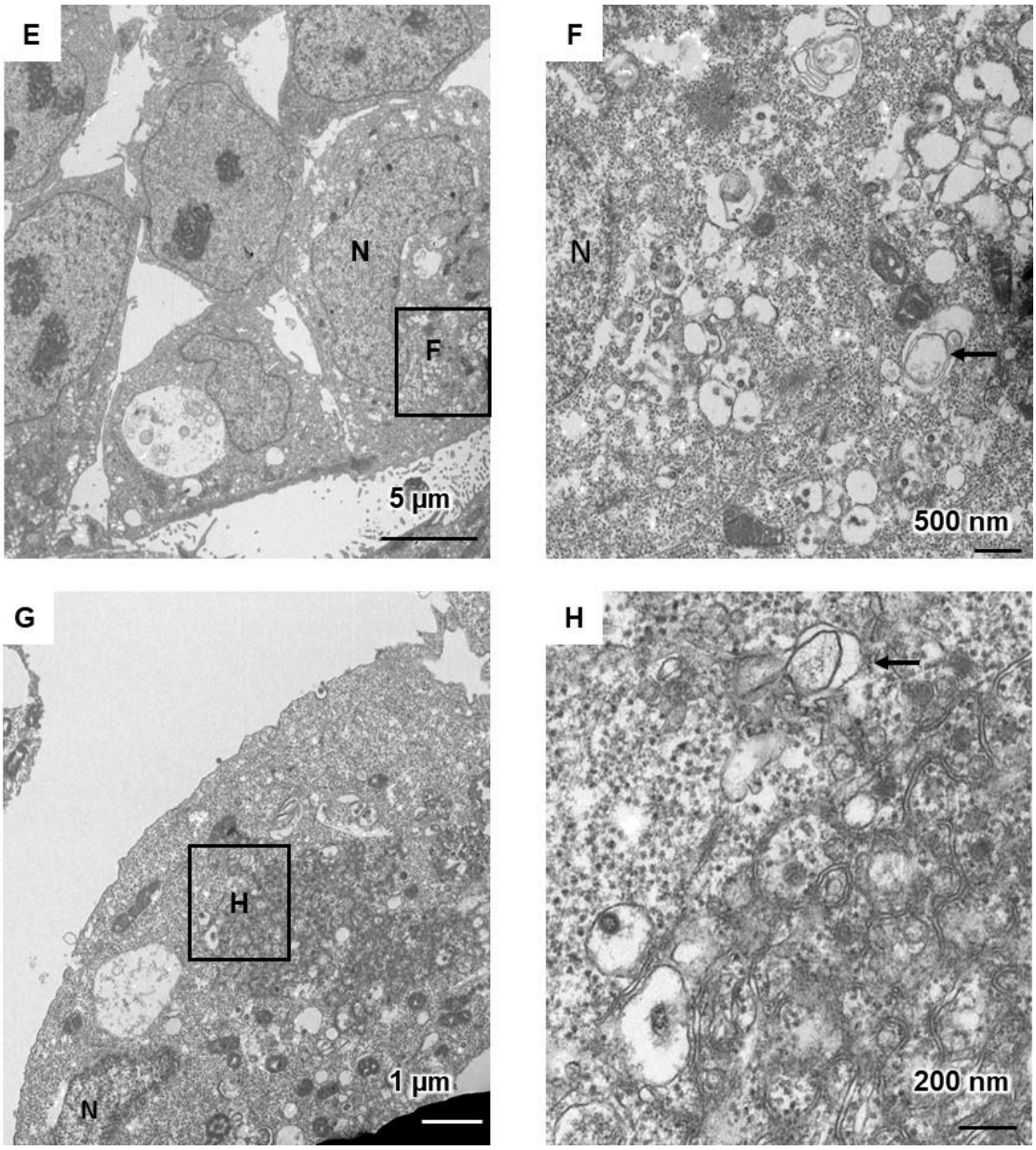

Figure S3　TEM images of infected ACE2-iPS cells, Related to Figure 2

(**A-D**) Endoplasmic reticulum-Golgi intermediate compartment (ERGIC) containing SARS-CoV-2 particles (black arrows) was observed in infected ACE2-iPS cells. (**E-H**) Double membrane vesicles (black arrows) were observed in infected ACE2-iPS cells.

Figure S4

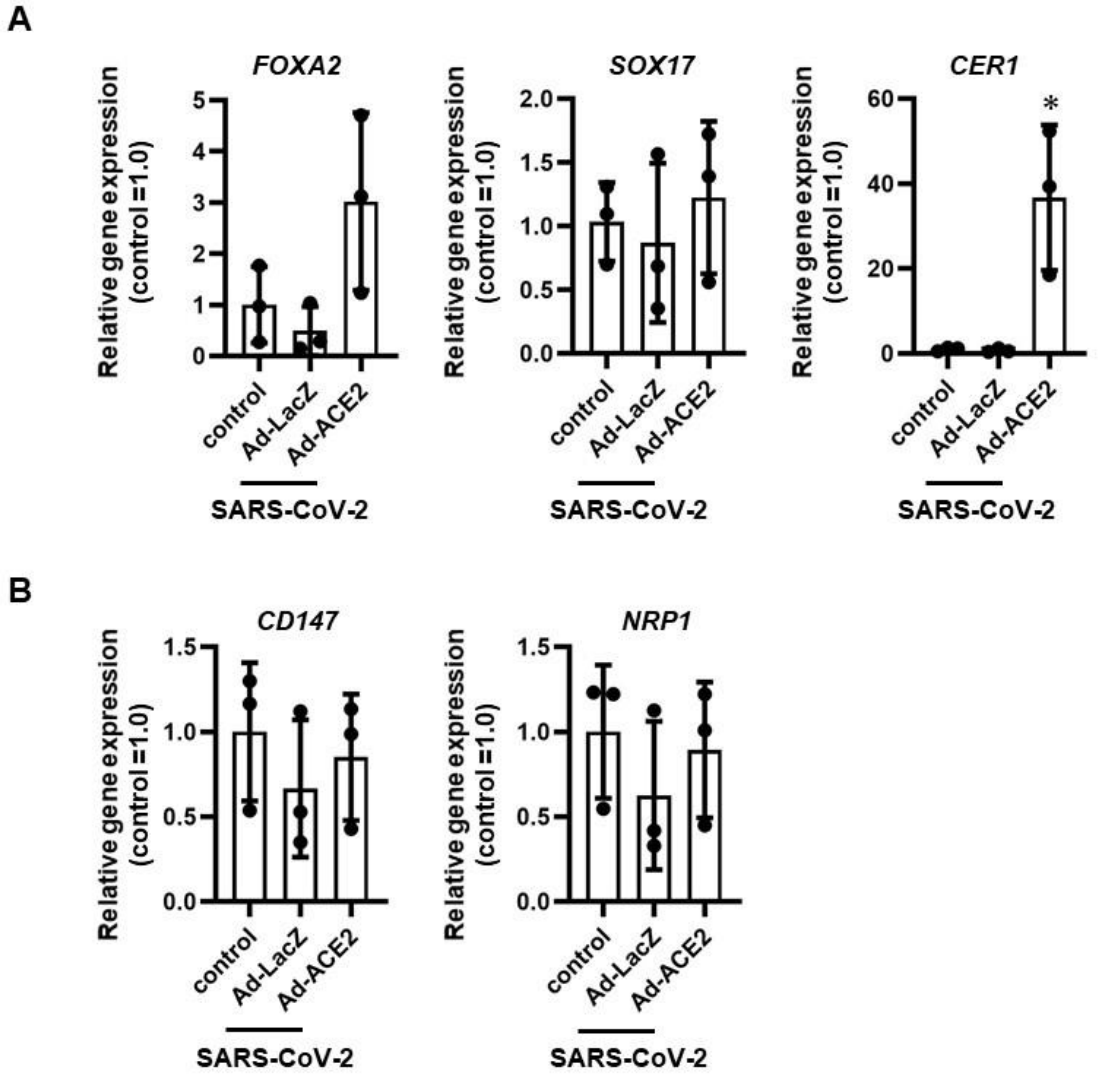

Figure S4　Gene expression profiles of differentiation markers and viral receptors in infected ACE2-iPS cells, Related to Figure 3

Undifferentiated human iPS cells (1383D6) were transduced with 600 VP/cell of LacZ- or ACE2-expressing Ad vectors (Ad-LacZ and Ad-ACE2, respectively) for 2 hr and then cultured with AK02 medium for 2 days. Control human iPS cells were not transduced with Ad vectors. The LacZ- and ACE2-expressing human iPS cells were then infected with SARS-CoV-2 (5×10^4 TCID50/well) for 2 hr and cultured with AK02 medium for 3 days. (**A, B**) The gene expression levels of endoderm markers (*FOXA2*, *SOX17*, and *CER1*) (**A**) and viral receptors (*CD147* and *NRP1*) (**B**) were examined by qPCR. Data are represented as means ± SD (n=3). One-way ANOVA followed by Tukey's post hoc test (*p<0.05, compared with Ad-LacZ).

Figure S5

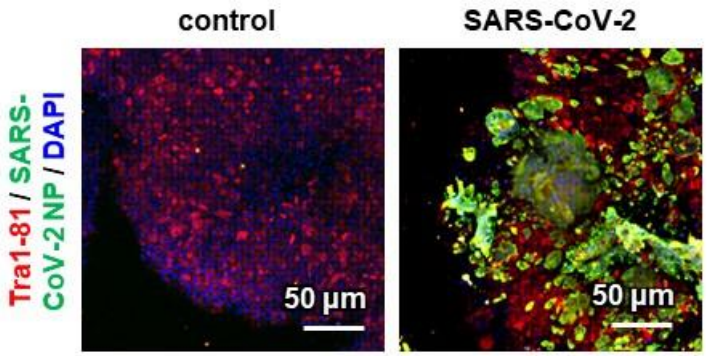

Figure S5　Immunofluorescence analysis of infected ACE2-iPS cells, Related to Figure 3

Immunofluorescence analysis of SARS-CoV-2 NP (green) and OCT3/4 (red) in uninfected and infected ACE2-iPS cells. Nuclei were counterstained with DAPI (blue).

Figure S6

A

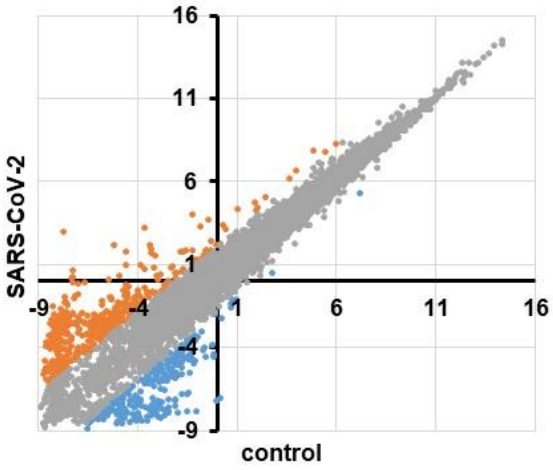

Dot	Description	Count	Rate (%)
	Detected	19370	
●	Up-regulated	792	4.1
●	Down-regulated	494	2.6
●	No change	18084	93.4

B

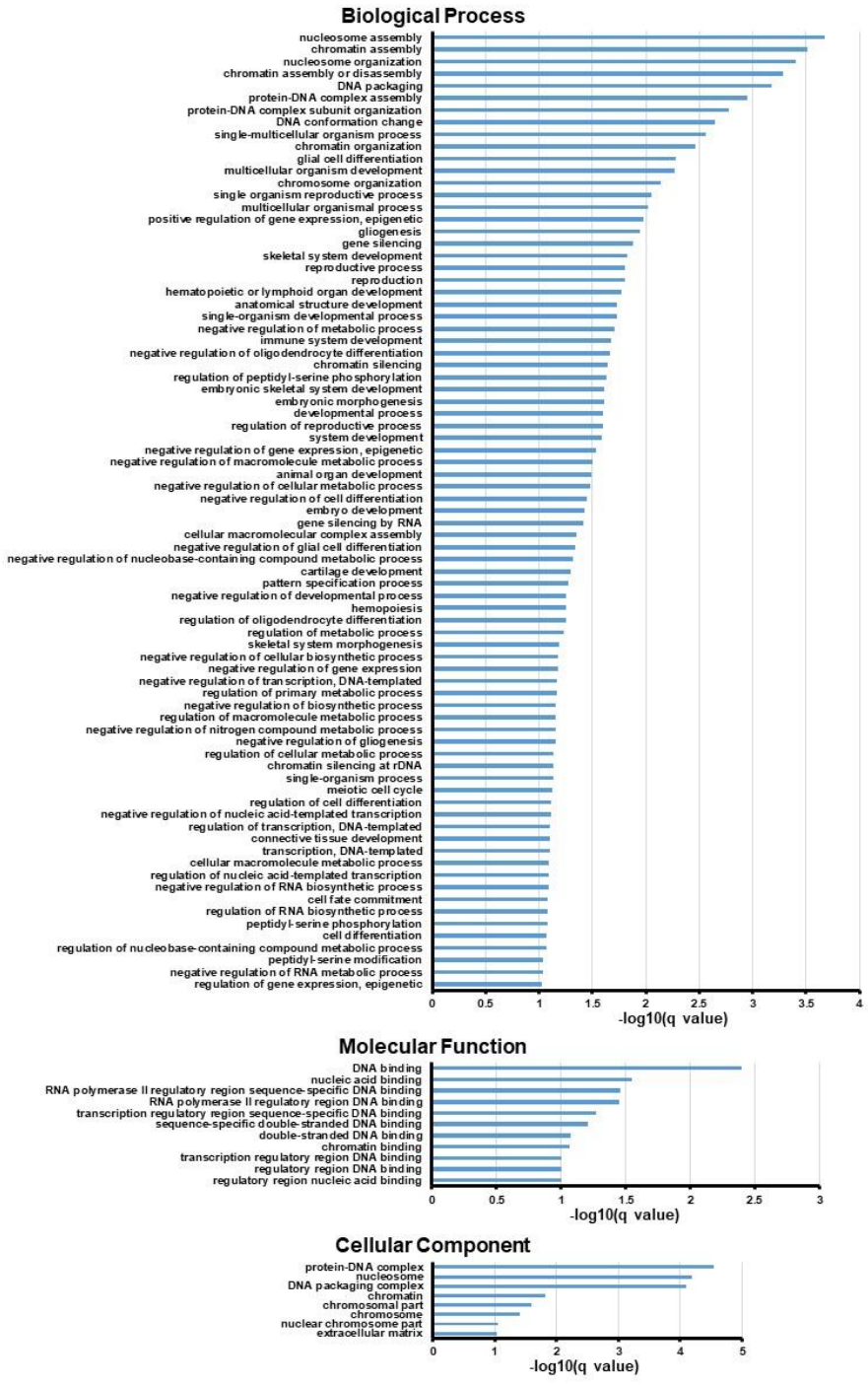
Biological Process
nucleosome assembly
chromatin assembly
nucleosome organization
chromatin assembly or disassembly
DNA packaging
protein-DNA complex assembly
protein-DNA complex subunit organization
DNA conformation change
single-multicellular organism process
chromatin organization
glial cell differentiation
multicellular organism development
chromosome organization
single organism reproductive process
multicellular organismal process
positive regulation of gene expression, epigenetic
gliogenesis
gene silencing
skeletal system development
reproductive process
reproduction
hematopoietic or lymphoid organ development
anatomical structure development
single-organism developmental process
negative regulation of metabolic process
immune system development
negative regulation of oligodendrocyte differentiation
chromatin silencing
regulation of peptidyl-serine phosphorylation
embryonic skeletal system development
embryonic morphogenesis
developmental process
regulation of reproductive process
system development
negative regulation of gene expression, epigenetic
negative regulation of macromolecule metabolic process
animal organ development
negative regulation of cellular metabolic process
negative regulation of cell differentiation
embryo development
gene silencing by RNA
cellular macromolecular complex assembly
negative regulation of glial cell differentiation
negative regulation of nucleobase-containing compound metabolic process
cartilage development
pattern specification process
negative regulation of developmental process
hemopoiesis
regulation of oligodendrocyte differentiation
regulation of metabolic process
skeletal system morphogenesis
negative regulation of cellular biosynthetic process
negative regulation of gene expression
negative regulation of transcription, DNA-templated
regulation of primary metabolic process
negative regulation of biosynthetic process
regulation of macromolecule metabolic process
negative regulation of nitrogen compound metabolic process
negative regulation of gliogenesis
regulation of cellular metabolic process
chromatin silencing at rDNA
single-organism process
meiotic cell cycle
regulation of cell differentiation
negative regulation of nucleic acid-templated transcription
regulation of transcription, DNA-templated
connective tissue development
transcription, DNA-templated
cellular macromolecule metabolic process
regulation of nucleic acid-templated transcription
negative regulation of RNA biosynthetic process
cell fate commitment
regulation of RNA biosynthetic process
peptidyl-serine phosphorylation
cell differentiation
regulation of nucleobase-containing compound metabolic process
peptidyl-serine modification
negative regulation of RNA metabolic process
regulation of gene expression, epigenetic
0
0.5
1
1.5
2
2.5
3
3.5
4
-log10(q value)
Molecular Function
DNA binding
nucleic acid binding
RNA polymerase II regulatory region sequence-specific DNA binding
RNA polymerase II regulatory region DNA binding
transcription regulatory region sequence-specific DNA binding
sequence-specific double-stranded DNA binding
double-stranded DNA binding
chromatin binding
transcription regulatory region DNA binding
regulatory region DNA binding
regulatory region nucleic acid binding
0
0.5
1
1.5
2
2.5
3
-log10(q value)
Cellular Component
protein-DNA complex
nucleosome
DNA packaging complex
chromatin
chromosomal part
chromosome
nuclear chromosome part
extracellular matrix
0
1
2
3
4
5
-log10(q value)

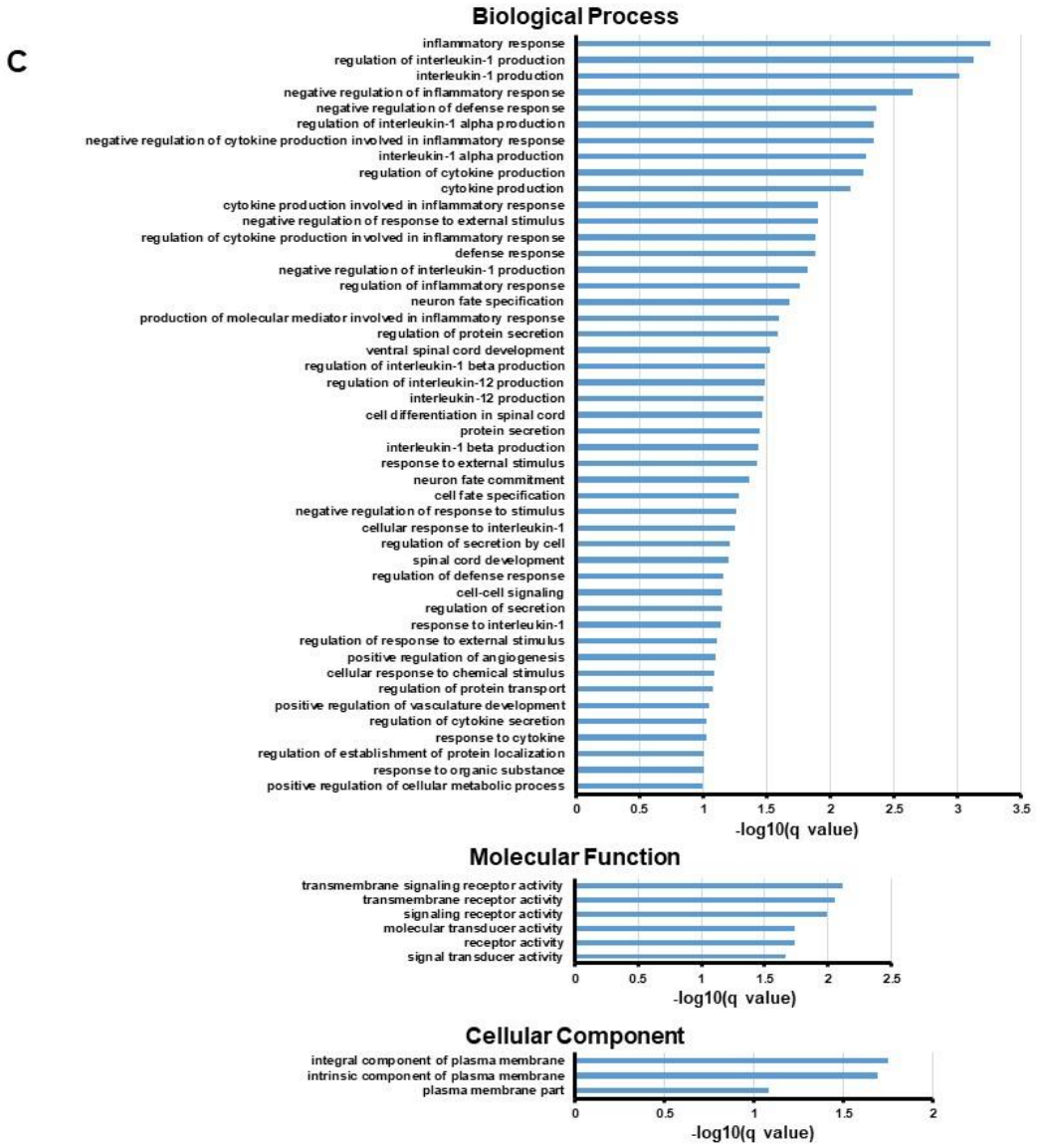

Figure S6　Global gene expression analysis of infected ACE2-iPS cells, Related to Figure 4

RNA-seq analysis of uninfected and infected ACE2-iPS cells. (**A**) A scatter plot of uninfected ACE2-iPS cells (control) vs. infected ACE2-iPS cells (SARS-CoV-2). The count and rate of up-regulated and down-regulated genes are summarized in the table. (**B, C**) GO analysis was performed for gene sets whose gene expression levels were decreased (**B**) or increased (**C**) more than three-fold.

Figure S7

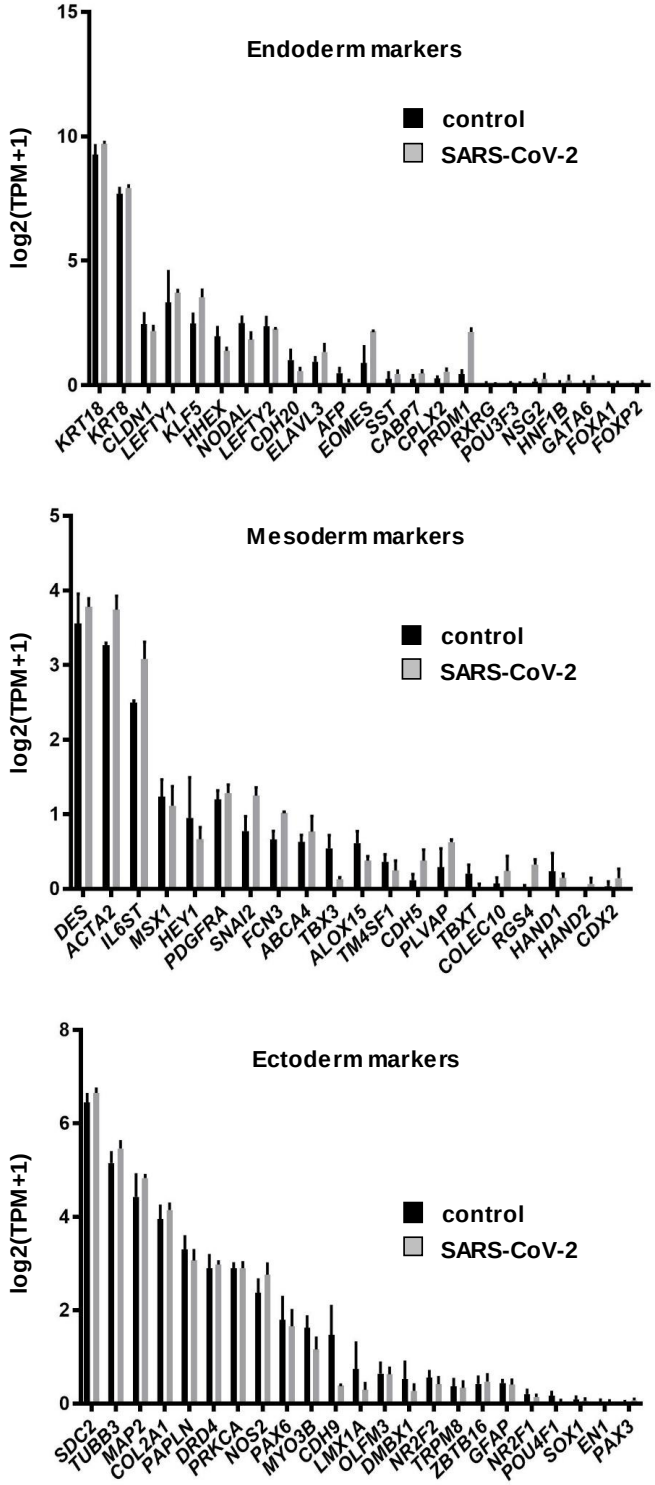

Figure S7 Gene expression profiles of endoderm, mesoderm, and ectoderm markers in infected ACE2-iPS cells, Related to Figure 4

RNA-seq analysis of uninfected and infected ACE2-iPS cells. Bar plots of ectoderm, mesoderm, and endoderm markers in uninfected ACE2-iPS cells (control) and infected ACE2-iPS cells (SARS-CoV-2) are shown.

Supplemental tables

Table S1 Drugs used in the infection experiments, Related to Figure 6

Drug	Catalogue	Company
Camostat mesylate	SML0057	Sigma-Aldrich
Chloroquine diphosphate	No.4109	Tocris
EIDD-2801	HY-135853	MedChemExpress
Favipiravir	S7975	Selleck Chemicals
Ivermectin	I8618	LKT Labs
Nafamostat mesylate	N0289-10MG	Sigma-Aldrich
Recombinant human IFN-β	300-02BC	PeproTech
Remdesivir	A17170	Clinisciences

Table S2 Primers used in this study, Related to Figures 3, 6, S1, S2, and S4

Gene name	Fwd primer	Rev primer
ACE2	ACAGTCCACACTTGCCCAAAT	TGAGAGCACTGAAGACCCATT
CD147	GAAGTCGTCAGAACACATCAACG	TTCCGGCGCTTCTCGTAGA
CER1	ACAGTGCCCTTCAGCCAGACT	ACAACTACTTTTTCACAGCCTTCGT
FOXA2	GCGACCCCAAGACCTACAG	GGTTCTGCCGGTAGAAGGG
GAPDH	GGAGCGAGATCCCTCCAAAAT	GGCTGTTGTCATACTTCTCATGG
IFNα	GCCTCGCCCTTTGCTTTACT	CTGTGGGTCTCAGGGAGATCA
IFNβ	ATGACCAACAAGTGTCTCCTCC	GGAATCCAAGCAAGTTGTAGCTC
ISG15	CGCAGATCACCCAGAAGATCG	TTCGTCGCATTTGTCCACCA
NANOG	AGAAGGCCTCAGCACCTAC	GGCCTGATTGTTCCAGGATT
NRP1	GGCGCTTTTCGCAACGATAAA	TCGCATTTTTCACTTGGGTGAT
OCT3/4	CTTGAATCCCGAATGGAAAGGG	GTGTATATCCCAGGGTGATCCTC
SARS-CoV-N	CCAGGTAACAAACCAACCAACTTTCG	GGTTACTGCCAGTTGAATCTGAGG
SOX17	GTGGACCGCACGGAATTTG	GAGGCCCATCTCAGGCTTG
SOX2	GGCAGCTACAGCATGATGATGCAGGAGC	CTGGTCATGGAGTTGTACTGCAGG
TMPRSS2	GTCCCCACTGTCTACGAGGT	CAGACGACGGGGTTGGAAG

Table S3 Antibodies used in this study, Related to Figures 3, S2, and S5

Antigen	Catalogue	Host	Company
Donkey anti-Mouse IgG (H+L) Highly Cross-Adsorbed Secondary Antibody, Alexa Fluor Plus 594	A32744	Donkey	Thermo Fisher Scientific
Goat anti-Rabbit IgG (H+L) Highly Cross-Adsorbed Secondary Antibody, Alexa Fluor Plus 488	A32731	Goat	Thermo Fisher Scientific
OCT3/4	sc-5279	Mouse	Santa Cruz Biotechnology
SARS-CoV-2 NP	A2061-50	Rabbit	BIO Vision
SOX2	sc-365823	Mouse	Santa Cruz Biotechnology
Tra1-81	MAB4381	Mouse	Sigma-Aldrich

Transparent methods

Materials availability

All unique/stable reagents generated in this study are available from the corresponding authors with a completed Materials Transfer Agreement.

Human ES/iPS cells

The human ES/iPS cell lines 1383D6 (Nakagawa et al., 2014) (provided by Dr. Masato Nakawaga, Kyoto University), 201B7 (Takahashi et al., 2007), Tic (JCRB1331, JCRB Cell Bank), H1 (WA01), H9 (WA09) (WiCell Research Institute), KhES1, KhES2, and KhES3 (Kyoto University) were maintained on 0.5 μg/cm^2 recombinant human laminin 511 E8 fragments (iMatrix-511, Nippi) with StemFit AK02N medium (Ajinomoto) containing 10 μM Y-27632 (from day 0 to day 1, FUJIFILM Wako Pure Chemical). To passage human ES/iPS cells, near-confluent human ES/iPS cell colonies were treated with TrypLE Select Enzyme (Thermo Fisher Scientific) for 5 min at 37°C. After the centrifugation, the cells were seeded at an appropriate cell density (1.3×10^4 cells/9 cm^2) onto iMatrix-511 and subcultured every 6 days. Human ES cells were used following the Guidelines for Derivation and Utilization of Human Embryonic Stem Cells of the Ministry of Education, Culture, Sports, Science and Technology of Japan, and the study was approved by an independent ethics committee. Except for **figure 6**, the human iPS cell line 1383D6 was used for all experiments.

SARS-CoV-2 preparation

The SARS-CoV-2 strains used in this study (SARS-CoV-2/Hu/DP/Kng/19-027) were provided by the Kanagawa Prefectural Institute of Public Health. SARS-CoV-2 was isolated from a COVID-19 patient (GenBank: LC528233.1). The isolation and analysis of the virus will be described elsewhere (manuscript in preparation). The virus was plaque-purified and propagated in Vero cells and stored at -80°C. All experiments including virus infections were done in a biosafety level 3 facility at Kyoto University strictly following regulations.

Adenovirus vectors

Ad vectors were constructed using Adeno-X^{TM} Adenoviral System 3 (Takara Bio). The ACE2 and TMPRSS2 genes were amplified by PCR using cDNA generated from Pulmonary Alveolar Epithelial Cell Total RNA (ScienCell Research Laboratories) as a template. The ACE2 and TMPRSS2 genes were inserted into Adeno-X^{TM}

Adenoviral System 3, resulting in pAdX-ACE2 and pAdX-TMPRSS2, respectively. The ACE2- and TMPRSS2-expressing Ad vectors (Ad-ACE2 and Ad-TMPRSS2, respectively) were propagated in HEK293 cells (JCRB9068, JCRB Cell Bank). LacZ-expressing Ad vectors were purchased from Vector Biolabs. The vector particle (VP) titer was determined by using a spectrophotometric method (Maizel Jr et al., 1968).

Viral titration of SARS-CoV-2

Viral titers were measured by median tissue culture infectious dose (TCID50) assays at a biosafety level 3 laboratory (Kyoto University). TMPRSS2/Vero cells (JCRB1818, JCRB Cell Bank) (Matsuyama et al., 2020) were cultured with Minimum Essential Media (MEM, Sigma-Aldrich) supplemented with 5% fetal bovine serum (FBS), and 1% penicillin/streptomycin and seeded into 96-well cell culture plates (Thermo Fisher Scientific). The samples were serially diluted 10-fold from 10^{-1} to 10^{-8} in the cell culture medium. Dilutions were placed onto the TMPRSS2/Vero cells in triplicate and incubated at 37°C for 96 hr. Cytopathic effects were evaluated under a microscope. TCID50/mL was calculated using the Reed-Muench method.

Quantification of viral RNA copy number

The cell culture supernatant was mixed with an equal volume of 2×RNA lysis buffer (distilled water containing 0.4 U/uL SUPERase I^{TM} RNase Inhibitor (Thermo Fisher Scientific), 2% Triton X-100, 50 mM KCl, 100 mM Tris-HCl (pH 7.4), and 40% glycerol) and incubated at room temperature for 10 min. The mixture was diluted 10 times with distilled water. Viral RNA was quantified using a One Step TB Green PrimeScript PLUS RT-PCR Kit (Perfect Real Time) (Takara Bio) on a StepOnePlus real-time PCR system (Thermo Fisher Scientific). The primers used in this experiment are as follows: (forward) AGCCTCTTCTCGTTCCTCATCAC and (reverse) CCGCCATTGCCAGCCATTC. Standard curves were prepared using SARS-CoV-2 RNA (10^5 copies/μL) purchased from Nihon Gene Research Laboratories.

Ultrathin section transmission electron microscopy (TEM)

Uninfected and infected ACE2-iPS cells were fixed with 2.5% glutaraldehyde in 0.1M cacodylate buffer and subsequently post-fixed with 1% osmium tetroxide in the same buffer for 1 hr at 4°C. After fixation, they were dehydrated in a series of ethanol gradient and embedded in epoxy resin. Ultrathin sections were cut, stained with uranyl acetate and lead citrate, and examined using an electron microscope (HITACHI HT-7700) at 80 kV.

RNA-seq

Total RNA was prepared using an RNeasy Mini Kit (Qiagen). RNA integrity was assessed with a 2100 Bioanalyzer (Agilent Technologies). The library preparation was performed using a TruSeq stranded mRNA sample prep kit (Illumina) according to the manufacturer's instructions. Sequencing was performed on an Illumina NextSeq500. The fastq files were generated using bcl2fastq-2.20. Adapter sequences and low-quality bases were trimmed from the raw reads by Cutadapt ver 1.14 (Martin, 2011). The trimmed reads were mapped to human reference genome sequences (hg38) using STAR ver 2.5.3a (Dobin et al., 2013) with the GENCODE (release 36, GRCh38.p13) (Frankish et al., 2019) gtf file. The raw counts for protein-coding genes were calculated using htseq-count ver. 0.12.4 (Anders et al., 2015) with the GENCODE gtf file. Gene expression levels were determined as transcripts per million (TPM) with DEseq2 (Love et al., 2014). Raw data concerning this study were submitted under Gene Expression Omnibus (GEO) accession number GSE166990.

SARS-CoV-2 infection and drug treatment

ACE2-iPS cells and Vero cells (JCRB0111, JCRB Cell Bank) cultured in a 96-well plate (2.0×10^4 cells/well) were infected with 2.0×10^3 TCID50/well of SARS-CoV-2 for 2 hr and then cultured with medium containing drugs. In the infection and drug treatment experiments, the medium containing drugs was replaced with fresh medium every day. At day 2 (Vero cells) or day 4 (ACE2-iPS cells) after the infection, the viral RNA copy number in the cell culture supernatant was measured by qPCR. Drugs used in the infection experiments are summarized in **Table S1**.

Quantitative PCR

Total RNA was isolated from human iPS cells using ISOGENE (NIPPON GENE). cDNA was synthesized using 500 ng of total RNA with a Superscript VILO cDNA Synthesis Kit (Thermo Fisher Scientific). Real-time RT-PCR was performed with SYBR Green PCR Master Mix (Thermo Fisher Scientific) using a StepOnePlus real-time PCR system (Thermo Fisher Scientific). The relative quantitation of target mRNA levels was performed by using the $2^{-\Delta\Delta CT}$ method. The values were normalized by those of the housekeeping gene, *glyceraldehyde 3-phosphate dehydrogenase* (*GAPDH*). The PCR primer sequences are shown in **Table S2**.

Immunofluorescence staining

For the immunofluorescence staining of human iPS cells, the cells were fixed with 4% paraformaldehyde in PBS at 4°C. After blocking the cells with PBS containing 2% bovine serum albumin and 0.2% Triton X-100 at room temperature for 45 min, the cells were incubated with a primary antibody at 4°C overnight and then with a secondary antibody at room temperature for 1 hr. All antibodies used in this report are described in **Table S3**.

Statistical analyses

Statistical significance was evaluated by unpaired two-tailed Student's *t*-test or one-way analysis of variance (ANOVA) followed by Tukey's post hoc tests. Statistical analyses were performed using GraphPad Prism8 and 9. Data are representative of three independent experiments. Details are described in the figure legends.

Supplemental references

Anders, S., Pyl, P.T., and Huber, W. (2015). HTSeq—a Python framework to work with high-throughput sequencing data. Bioinformatics *31*, 166-169.

Dobin, A., Davis, C.A., Schlesinger, F., Drenkow, J., Zaleski, C., Jha, S., Batut, P., Chaisson, M., and Gingeras, T.R. (2013). STAR: ultrafast universal RNA-seq aligner. Bioinformatics *29*, 15-21.

Frankish, A., Diekhans, M., Ferreira, A.-M., Johnson, R., Jungreis, I., Loveland, J., Mudge, J.M., Sisu, C., Wright, J., and Armstrong, J. (2019). GENCODE reference annotation for the human and mouse genomes. Nucleic acids research *47*, D766-D773.

Love, M.I., Huber, W., and Anders, S. (2014). Moderated estimation of fold change and dispersion for RNA-seq data with DESeq2. Genome biology *15*, 1-21.

Maizel Jr, J.V., White, D.O., and Scharff, M.D. (1968). The polypeptides of adenovirus: I. Evidence for multiple protein components in the virion and a comparison of types 2, 7A, and 12. Virology *36*, 115-125.

Martin, M. (2011). Cutadapt removes adapter sequences from high-throughput sequencing reads. EMBnet journal *17*, 10-12.

Matsuyama, S., Nao, N., Shirato, K., Kawase, M., Saito, S., Takayama, I., Nagata, N., Sekizuka, T., Katoh, H., and Kato, F. (2020). Enhanced isolation of SARS-CoV-2 by TMPRSS2-expressing cells. Proceedings of the National Academy of Sciences *117*, 7001-7003.

Nakagawa, M., Taniguchi, Y., Senda, S., Takizawa, N., Ichisaka, T., Asano, K., Morizane, A., Doi, D., Takahashi, J., and Nishizawa, M. (2014). A novel efficient feeder-free culture system for the derivation of human induced pluripotent stem cells. Scientific reports *4*, 1-7.

Takahashi, K., Tanabe, K., Ohnuki, M., Narita, M., Ichisaka, T., Tomoda, K., and Yamanaka, S. (2007). Induction of pluripotent stem cells from adult human fibroblasts by defined factors. cell *131*, 861-872.